PAPER

Fabrication of plasmonic devices using femtosecond laser-induced forward transfer technique

Nanotechnology **23** (2012) 444013 (9pp) doi:10.1088/0957-4484/23/44/444013

Fabrication of plasmonic devices using femtosecond laser-induced forward transfer technique

Ming Lun Tseng[1], Chia Min Chang[2,3], Bo Han Chen[1], Yao-Wei Huang[1], Cheng Hung Chu[3,4], Kuang Sheng Chung[3], Yen Ju Liu[1], Hung Guei Tsai[3], Nien-Nan Chu[5], Ding-Wei Huang[2], Hai-Pang Chiang[4,5] and Din Ping Tsai[1,3,5,6]

[1] Graduate Institute of Applied Physics, National Taiwan University, Taipei 106, Taiwan
[2] Institute of Photonics and Optoelectronics, National Taiwan University, Taipei 106, Taiwan
[3] Department of Physics, National Taiwan University, Taipei 106, Taiwan
[4] Institute of Optoelectronic Sciences, National Taiwan Ocean University, Keelung 202, Taiwan
[5] Instrument Technology Research Center, National Applied Research Laboratories, Hsinchu 300, Taiwan
[6] Research Center for Applied Sciences, Academia Sinica, Taipei 115, Taiwan

E-mail: dptsai@phys.ntu.edu.tw

Received 6 March 2012, in final form 2 May 2012
Published 18 October 2012
Online at stacks.iop.org/Nano/23/444013

Abstract
Using femtosecond laser-induced forward transfer techniques we have fabricated gold dots and nanoparticles on glass substrates, as well as nanobumps on gold thin film. The surface morphologies of these structures with different laser fluences and film thicknesses are investigated. We also study the focusing and defocusing properties of the nanofence—an arranged nanobump pattern—by the total-internal reflection microscope. Observations reveal that surface plasmon waves can be highly directed and focused via this nanofence pattern. Results are in good agreement with the simulation results using the finite-element method and demonstrate the potential applications of these nanophotonic devices. Furthermore, we utilize high laser energy to fabricate plasmonic waveguides, and also succeed in transferring the waveguides to another substrate. The attenuation rates of the light propagating in the waveguides are observed to achieve 0.31 dB μm^{-1} and 0.48 dB μm^{-1} on the target and receiver sides, respectively.

(Some figures may appear in colour only in the online journal)

1. Introduction

The laser direct-writing (LDW) technique has attracted a particular interest of researchers in surface patterning applications on micrometer and nanometer scales [1–10]. This technique offers significant advantages in terms of processing speed and simplicity with high throughput, which is much faster than other maskless fabrication techniques [11–14]. Being focused on the pre-coated materials on substrates, the laser beam as a burin can ablate (or functionalize) the illuminated material rapidly, and the designed devices can be made on the substrate [15, 16]. This one-step technique, both time-saving and cost efficient, can help people save a lot of budget and time [6–8]. Also, the recent rapid progress of ultrafast lasers brings new possibilities for fundamental understanding of the micro- and nanoscale material process [15–17]. The reason for using ultrafast laser pulses is primarily conditioned by their property of minimizing the heat-affected zones during the laser–material interaction compared to the longer nanosecond pulse durations [17]. Due to the rapid energy delivery (ultrafast material excitation) and the precision in controlling

the deposited energy, the femtosecond (fs) lasers have been treated as a useful tool in the surface or volume structure fabricating process for many different materials. By controlling the incident laser energy slightly below the ablation threshold of the adopted thin film, many interesting nanostructures such as microbumps and nanojets can be created on the surface [18–20].

Moreover, an additive LDW technique is the laser-induced forward transfer (LIFT) method [18, 21]. A schematic diagram of the LIFT setup is shown in figure 1. The laser beam is utilized to selectively remove the illuminated thin film (the target film) material from a transparent substrate and eventually forward transfer it onto another substrate (a receiver). In the process of LIFT, heat diffusion in the lateral direction of the exposed material will induce an increase of area in laser ablation, which leads to a decrease of fabrication resolution and flatness in the boundary region of fabricated structures. It is thus very important to minimize the heat-affected zones during the process of laser–material interaction. When the laser beam passing through the transparent substrate and focused on the pre-coated film is denoted as the donor, an expansive pressure at the interface between the film and the substrate will be created. The donor will melt and expand during exposure until the pressure is beyond the threshold to detach and transfer the material. The melting region of material is thus ablated forward and deposited onto the opposite substrate, denoted as the receiver. Since the pulse-width of a femtosecond laser is much smaller than that of a nanosecond laser, the heat-affected zones and the amounts of transferred materials in femtosecond LIFT will therefore be much smaller than that in nanosecond LIFT [17]. This accounts for why the transfer results of femtosecond LIFT will be better than that of nanosecond LIFT. LIFT techniques have become important direct-write alternatives to lithographic processes for generating high resolution and high throughput patterns, and have been successfully applied to process various materials (e.g. metals [22–26], phase-change chalcogenide material [18], biological materials [27], superconductors [28], and semiconductors [29]), and to fabricate nanophotonic devices (e.g. carbon nanotube field emission cathodes [30] and organic light-emitting diode pixels [31]).

With the progress in plasmonic nanophotonics, many techniques have been employed to fabricate metallic nanoparticles [20, 32–35] and plasmonic waveguides [36, 37]. Nanosphere lithography has been developed to fabricate nanoparticle arrays with high speed and low cost [34, 35], but shape and arrangement of the nanoparticles cannot be easily changed in this method. Focused ion-beams [36] and e-beams [37] have been used to fabricate integrated plasmonic components with precise shape and distance, but these lithographic methods suffer from limited processed area, expensive experimental setup, and long processing time. Recently, a localized surface plasmon polariton sensor composed of gold nanoparticles has been made on a flexible substrate by the LIFT technique [32]. Utilizing the LIFT technique to fabricate plasmonic nanoparticles arrays has great potential for 2D and 3D patterning [20] and

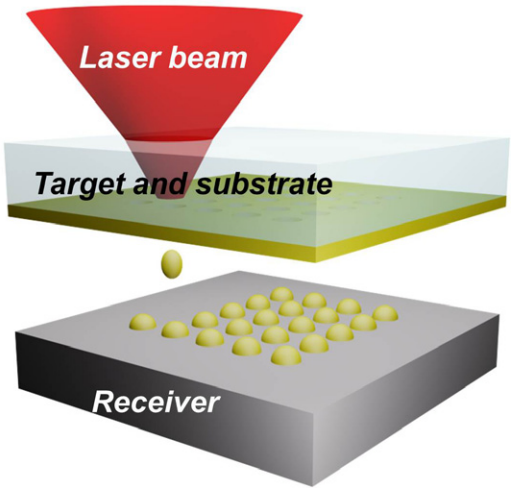

Figure 1. Schematic illustration of the LIFT technique.

plasmonic scattering devices [33]. However, except for a few examples mentioned above, fabrication of integrated plasmonic components by this technique has not yet been well developed. It is the purpose of our work to extend the LIFT technique to the fabrication of plasmonic structures and plasmonic waveguides. In this paper, various plasmonic structures are designed and fabricated on gold thin film and glass substrate with the femtosecond LIFT technique. The relationships between the formed structures and the input laser fluence under a broad range are studied. At the ablation threshold of gold thin films, gold nanoparticles on the receiver and the corresponding nanobumps on the target are obtained, respectively. The plasmonic devices composed of the gold nanobumps are designed and fabricated on gold thin films. Using this device, both the focusing and defocusing of the surface plasmon wave can be achieved. Finally, plasmonic waveguides of gold stripes are also made and studied.

2. Experimental details

The 'target' employed here is a gold thin film sputtered on a BK7 glass substrate (Matsunami cover glass, 22 × 22 mm^2, 0.15 mm thickness) under Ar pressure of 5 × 10^{-1} Pa by a conventional magnetron sputtering machine (Shibaura Mechatronics). Another BK7 glass is used as a 'receiver substrate'; see figure 1 inset. We have placed a 1 μm spacer between the receiver and target. Several spacing distances have been tried in our experiment, and the best transfer result was obtained by using 1 μm spacing. Spacing is a crucial parameter for feature resolution on the receiver. Too small or too large spacing will degrade the resolution on the receiver since the transferred materials from the donor should pass through a suitable distance before settling on the receiver. The sample is mounted on a nanometric computer controlled translation stage (Mad City Labs, Nano-LP200). The light source is an 800 nm wavelength Ti:sapphire laser beam (140 fs pulse duration and 80 MHz repetition rate; Coherent, Chameleon Ultra II). The exposure time, controlled by a shutter, is 30 ms for each shot, and an attenuator is used to

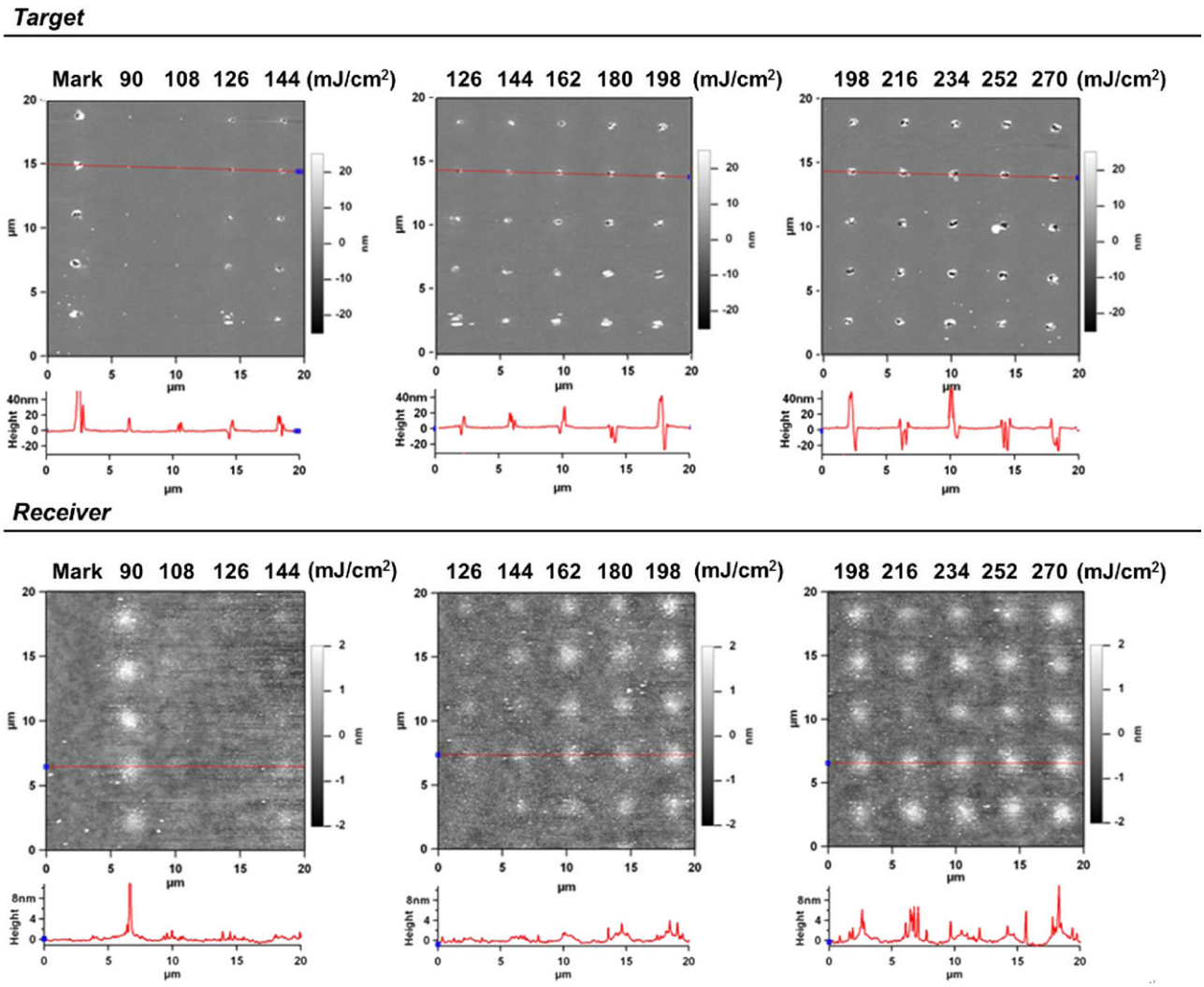

Figure 2. The transition of the fabricated structures with varying fs-laser fluence. The thickness of the gold film is set at 20 nm. (Up—target side; down—receiver side.) The laser fluence is increased from 90 to 270 mJ cm^{-2}. The first column, labelled 'mark', is used for the convenience of the alignment of the laser path.

modulate the incident fluence on the target. The applied laser fluence on the target is varied over a wide range between 90 and 342 mJ cm^{-2} for the study of the relationship between the fabricated structures and the laser fluence. All the structures shown in this paper are generated in a single shot, and the processes are carried out in air and at room temperature. Subsequently, characterization of surface morphology and pattern structure are carried out by using an atomic force microscope (AFM, Asylum Research, MFP-3D^{TM}).

3. Results and discussion

3.1. Nanobumps and nanoholes

Figure 2 shows the AFM images of the surface morphology on both the target and receiver sides. Each 'mark' is produced by a single laser shot. The incident laser fluence is varied from one column to another. The thicknesses of the gold films are set as 20 nm (figure 2), 30 nm (figure 3), and 40 nm (figure 4), respectively. Through observing the target and receiver sides, we can find two processing regimes, the nanobump corrugated surface and the crater-like morphology, and both of them have well defined laser fluence thresholds. In figure 2, the ablation threshold of a 20 nm thick gold thin film is found to be at $J_{th} = 126$ mJ cm^{-2}. As the laser fluence becomes higher than J_{th}, the illuminated part of the target film is ablated and elevated rims are observed. With increasing laser fluence, larger holes are obtained. In this region, the ablation process is usually accompanied by small bubbles growing on the gold thin film. This phenomenon is attributed to phase explosion [17, 19], which occurs mostly at the illuminated materials. Therefore, after laser transfer, deposited dots with island-like morphology nanoparticles can be formed on the receiver. Furthermore, when the laser fluence is slightly below the ablation threshold, gold nanobump structures on the target and gold nanoparticles on the receiver are observed, respectively. Similar results can also be observed with the thickness of the target at 30 nm and the ablation threshold at 198 mJ cm^{-2}; as well as at a target thickness of 40 nm and a threshold fluence of 306 mJ cm^{-2}, as shown in figures 3 and 4, respectively. Moreover, as shown in the target sides of figures

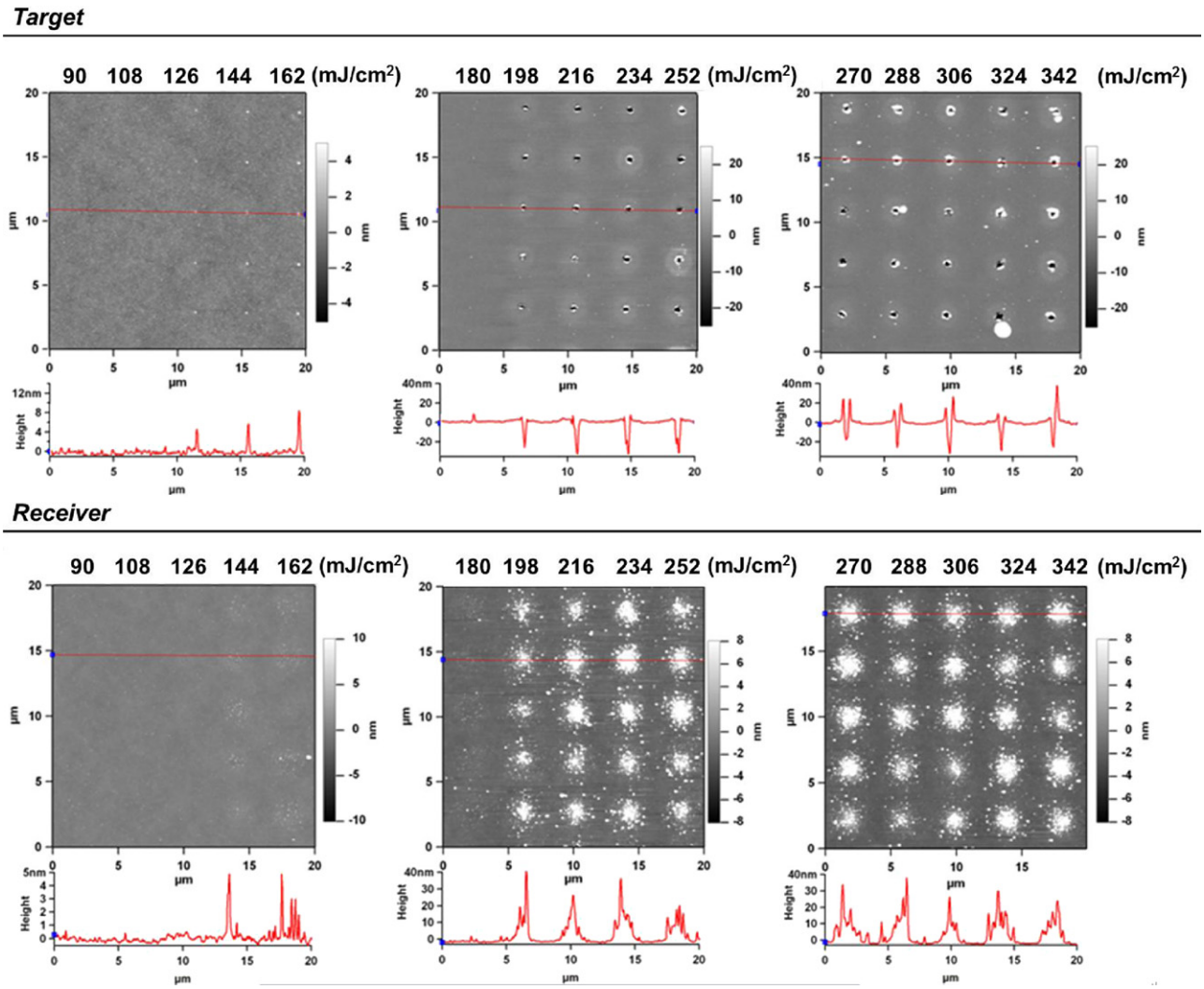

Figure 3. The transition of the fabricated structures with varying fs-laser fluence. The thickness of the gold films is set at 30 nm. The laser fluence is increased from 90 to 342 mJ cm^{-2}. (Up—target side; down—receiver side.)

3 and 4, some gold droplets are not transferred to the receiver and deposited beside the ablated holes on the target. From the AFM images of donors with laser exposure of 126 and 144 mJ cm^{-2}, there are bumps on the gold film but these are not entirely ablated. We therefore define the ablation threshold to be 198 mJ cm^{-2}, since the gold film was totally ablated at this stage.

We summarize our observations as follows: with different laser fluences applied to the gold thin films, different types of structure can be obtained on the target and receiver. For example, using a 30 nm thick gold thin film, with the laser fluence lower than the ablation threshold (198 mJ cm^{-2}), a cylindrical shaped nanobump with 18 nm height and 250 nm width is generated on the laser spot of the gold thin film; see figure 5(a). The formation of the gold nanobumps on the thin film is similar to our previous works [18, 38–40] Laser illumination induces melting and mass-redistribution of the gold material, accumulating the molten gold material at the center of the illuminated region. On the corresponding receiver, gold nanoparticles (5 nm height and 40 nm width in average) are observed. As the laser fluence is above the ablation threshold, the ablated crater is observed on the target side, and the transferred gold dot with 25 nm height and 1 μm diameter is obtained; see figure 5(b).

Moreover, according to our experimental results, the fluence thresholds for formation of nanobumps and ablated holes are seen to be proportional to the film thickness in the range of 20–40 nm with a step of 10 nm. Below the threshold fluence for nanobumps, no obvious structures are formed on the illuminated spots of the gold thin films. Between the thresholds of nanobump formation and laser-ablated hole formation, the gold nanobumps are formed on the surface of illuminated thin films, and the heights of the nanobumps are proportional to the applied laser fluence. Some gold nanoparticles are obtained on the corresponding receiver. Finally, above the ablated threshold, holes are formed on the gold thin films, and the ablated materials are transferred to the receiver surface. Furthermore, because the LIFT technique can transfer illuminated material onto arbitrary receivers such as flexible transparent sheets [41] and optical fibers [42], novel plasmonic applications with complex gold structures can be achieved by the LIFT technique with high efficiency.

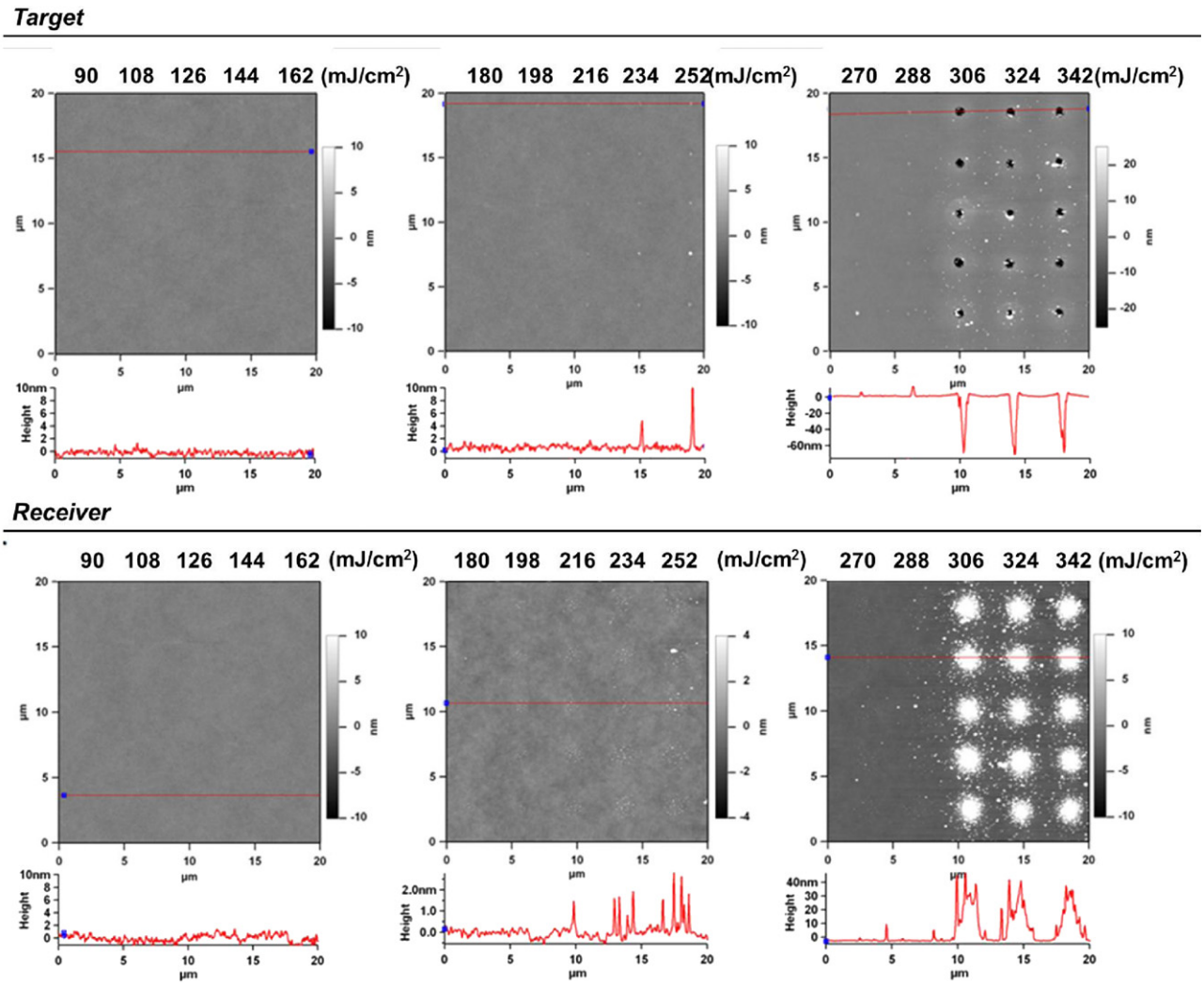

Figure 4. The transition of the *g* fabricated structures with varying fs-laser fluence. The thickness of the gold films is set at 40 nm, respectively. (Up—target side; down—receiver side.) The laser fluence is increased from 90 to 342 mJ cm^{-2}.

For example, the transferred gold nanoparticles and gold dots on the receiver are very useful in the applications of plasmonic thin film solar cells for efficient light trapping [43] and plasmonic photocatalysts for improving the efficiency of photocatalytic chemical reaction [44, 45].

3.2. Nanofence

By applying LDW technology, the morphology of thin film surface can be rapidly modified, hence providing an excellent shape-controlled and devisable capability for fabricating plasmonic devices on gold thin film. Here, the particular structures arranged by nanobumps are fabricated on the 30 nm thick gold thin film, and all of these nanobumps are fabricated with laser fluence 126 mJ cm^{-2}. As shown in figure 6(a), a quarter circle with radius of 5.7 μm is chosen to be a unit cell of this array with a period of 15 μm. Each of the quarter circles, as a nanofence, is composed of 21 nanobumps (averaged diameter of 250 nm) with an interspace of 450 nm for adjacent nanobumps, as shown in figure 6(b).

By using a total-internal reflection microscope (TIRM) with a high numerical aperture objective lens, which was used in our previous study [46], the surface plasmon polaritons (SPPs) are launched at the interface between air and gold by a green (532 nm) cw laser. A leaky wave into the optical far field can be generated by tunneling of SPPs from the air/gold thin film interface through the gold thin film, and can be collected by a charge-coupled digital camera (CCD) [47].

Figure 7 shows the images of leakage radiation from the interaction between SPPs and the nanofence patterns. The orientation of the nanofences as shown in figure 7(a) (figure 7(b)) is defined as concave (convex) relative to the propagation direction of the SPPs. We observed that the leakage radiation of SPPs scattered from the surface corrugations of the nanofence pattern is much stronger than that from the smooth metal surface of the gold film. In figure 7(a), three focal spots of the focusing pattern were observed, which implies that the SPPs were focused by a concave nanofence. In contrast, in figure 7(b) fringe patterns are observed, so they are defocused by a convex nanofence. These results may originate from the constructive interference of the SPP waves on the gold film.

For comparison with the experimental results, we simulate the interactions between nanofences and SPPs

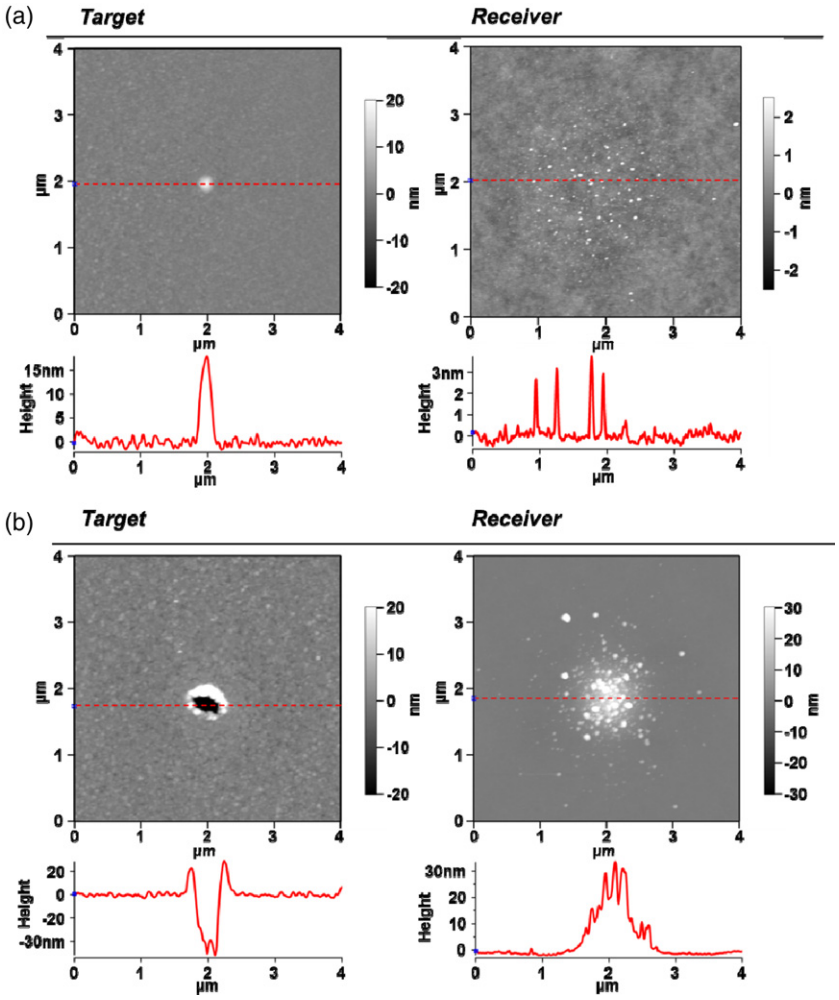

Figure 5. Two types of structure of LIFT gold 30 nm thick film. (a) 126 mJ cm^{-2} and (b) 198 mJ cm^{-2}.

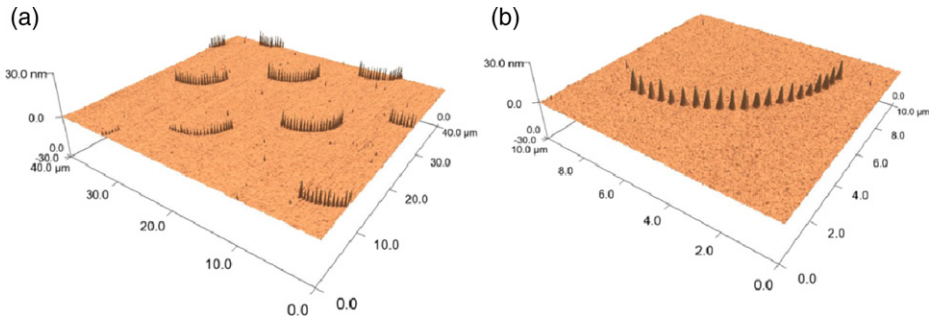

Figure 6. Three-dimensional AFM images of (a) the array arranged by quarter circles with a period of 15 μm and (b) the unit pattern of the array, composed of 21 nanobumps on a 30 nm gold film.

by the commercial program Comsol Multiphysics 3.5a, which is based on the finite-element method. The resonance wavelength of the SPPs on the flat gold/air interface is

$$\lambda_{spp} = \lambda_{in}\mathrm{Re}\sqrt{\frac{\varepsilon_{Au}+1}{\varepsilon_{Au}}}. \quad (1)$$

In our case, the incident wavelength, λ_{in}, is 532 nm, so the wavelength of the excited SPPs, λ_{spp}, is 469 nm, by using the dielectric constant of gold, $\varepsilon_{gold} = -4.4764 + 2.5318i$ [48].

Figures 8(a) and (b) are the two-dimensional simulation results of the time-averaged intensity for the two cases of the concave and convex nanofences, respectively. In figure 8(a), the three focusing spots are observed as well as in figure 7(a). Comparing figure 8(b) with figure 7(b), the fringe pattern is also observed. It is clear that these numerical results are exactly consistent with our experiment results. Consequently, one can achieve focusing or defocusing of an SPP using the nanofence structures.

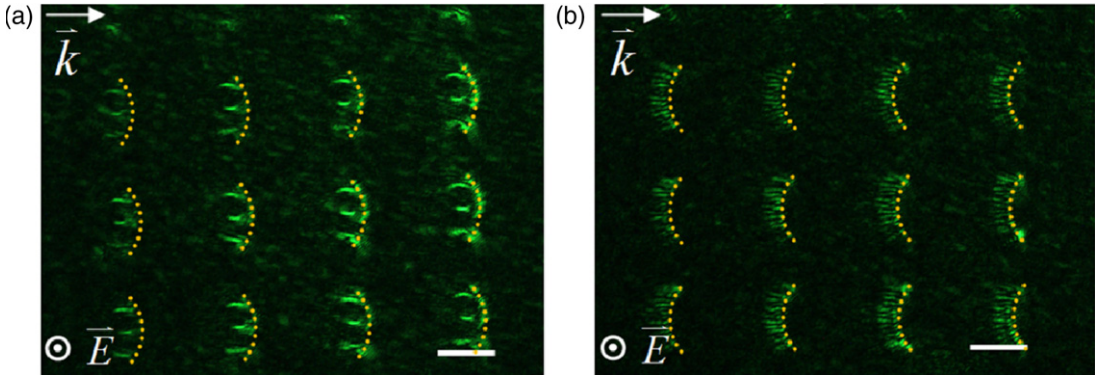

Figure 7. Dark field images of leakage radiation from SPPs scattered by (a) a concave nanofence and (b) a convex nanofence, which is marked by the yellow dotted curves. The wave vector of incident SPPs is along the horizontal direction. The scale bar is 10 μm. The dotted lines in yellow indicate the positions of the nanobump arrays.

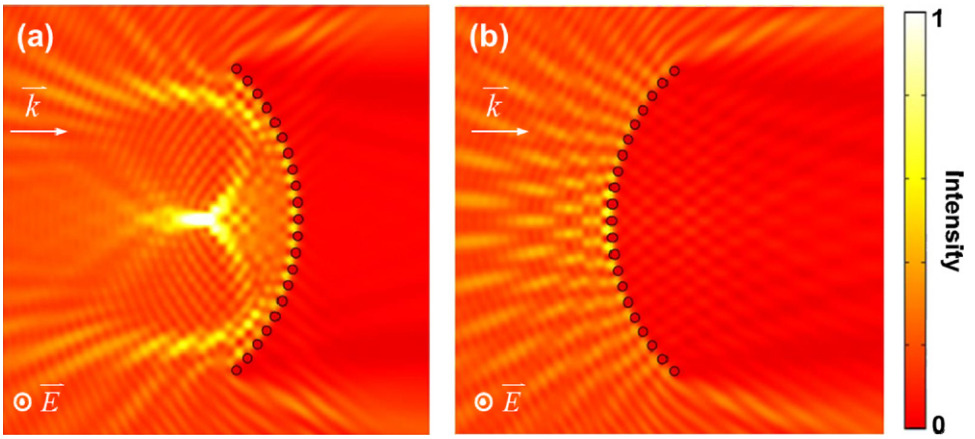

Figure 8. Simulated images of the time-averaged scattering intensity calculated by the finite-element method with the incident wavelength of SPPs at 469 nm. The SPP wave is incident from left to right.

3.3. Plasmonic waveguide

Since surface plasmon polaritons are light waves coupled to conduction electrons oscillating on a metal surface and can be laterally confined in the volume below the diffraction limit utilizing subwavelength waveguide structures, it is thus possible to couple light into a plasmonic waveguide that is smaller in cross section [49]. Here we use the LIFT technique to fabricate plasmonic waveguide structures both on 30 nm thick gold thin film and the receiver, as shown in figure 9. The gold thin film is scanned by the fs-laser beam of a rectangle path. The waveguides are fabricated with four different lengths: 10 μm, 15 μm, 20 μm, and 25 μm, respectively. After the process, gold stripes are obtained on the target (figure 9(a)), and the corresponding transferred gold structures are observed on the receiver (figure 9(b)). The width of the stripes on the target is around 400 nm, and the gap between the stripes and the thin film is around 480 nm. Also, SEM measurement shows that the width of the gold structures on the receiver is 480 nm, which is in good agreement with the gaps on the targets. We use a high numerical aperture microscope objective [50] to launch SPPs on the waveguides under a total-internal reflection (TIR) scheme. A 532 nm wavelength cw laser is employed to focus the input laser spots. As shown in figure 10, the emission light observed at the right end confirms that these structures (on both the target and the receiver) can be used as SPP waveguides. Two obvious light patterns can be observed at the two ends of the waveguides, which may be due to the relative roughness of the two ends, providing conditions for transforming the SPP waves into emitted light.

Figure 11 shows the ratio of the input intensity to the output intensity. According to Beer's law, the output intensity at the distance z can be expressed as

$$I(z) = I_0 \exp(-2z/d), \tag{2}$$

where I_0 is the input intensity, and d is the decay length. In our results, the decay lengths of the waveguides on the target and receiver sides are obtained to be 27.6 ± 2.8 μm and 17.8 ± 0.9 μm, respectively. Thus, the attenuations are 0.31 dB μm^{-1} (target side) and 0.48 dB μm^{-1} (receiver side).

4. Conclusion

In conclusion, various plasmonic structures have been fabricated and analyzed utilizing the femtosecond laser-induced forward transfer technique. The size and shape

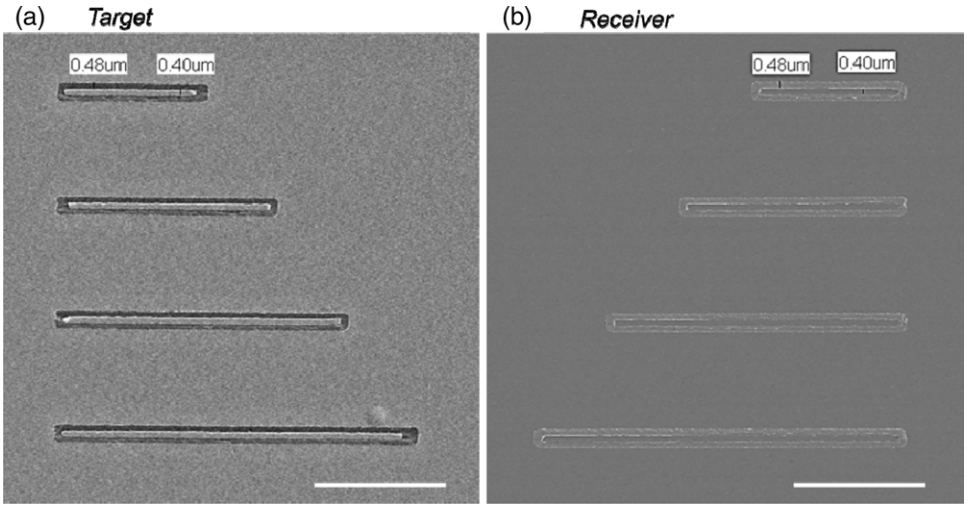

Figure 9. SEM images of (a) the fabricated gold stripes on the target and (b) the corresponding transferred gold structures on the receiver. The scale bar in the two pictures is 10 μm.

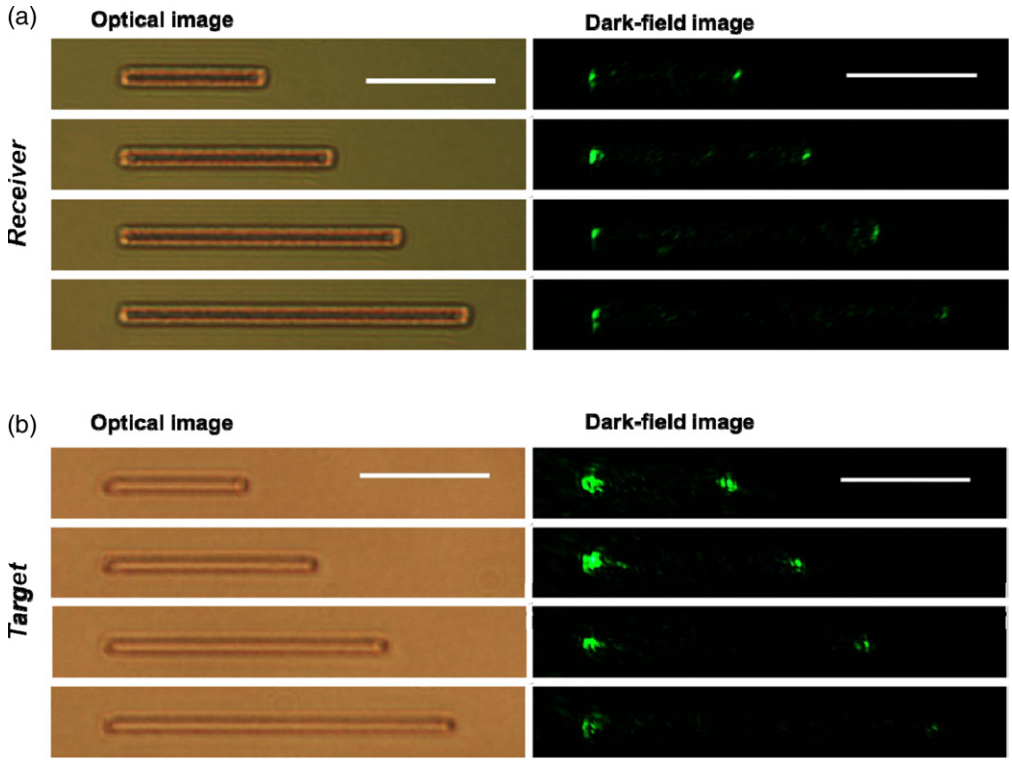

Figure 10. Optical microscope images of gold waveguide. (a) Target: left—optical transmission images of plasmonic waveguide structures with length 10 μm, 15 μm, 20 μm, and 25 μm, respectively. Right—dark-field images of gold waveguides exposed to through-prism TIR illumination of 532 nm cw laser. (b) Receiver side waveguides. The scale bar in all pictures is 10 μm.

of the transferred dots and nanoparticles obtained in this LIFT process can be controlled by the laser fluence and by the thickness of the target film. Gold stripes with various lengths are fabricated, which can be utilized as plasmonic waveguides. Moreover, when the laser fluence is slightly smaller than the ablation threshold of the thin film, nanobumps can be created on the gold thin film surface. An array composed of nanobumps can be used to modulate a surface plasmon wave on the gold thin film. The femtosecond LIFT technique has been proven as a flexible and versatile method for fabricating gold structures for plasmonic applications. This research has promising potential for areas such as photovoltaics, photocatalysts and integrated photonic circuits.

Acknowledgments

The authors acknowledge financial support from the National Science Council, Taiwan, under grant numbers 99-2120-M-002-012, 99-2911-I-002-127, 100-2120-M-002-008,

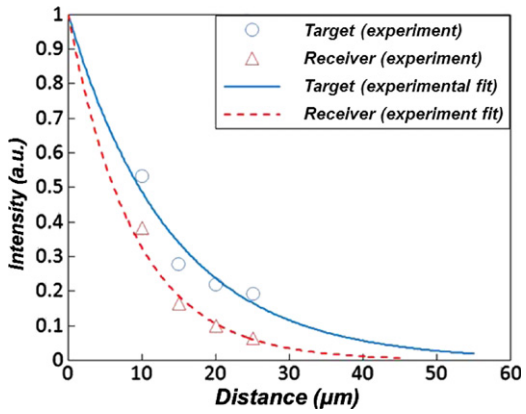

Figure 11. Plasmon intensity decay curves for gold waveguide of target and receiver sides under 532 nm excitation.

100-2923-M-002-007-MY3 and 100-2112-M-019-003-MY3, respectively. They are also grateful to the National Center for Theoretical Sciences, Taipei Office, the Molecular Imaging Center of National Taiwan University and the National Center for High-Performance Computing, Taiwan, for their support.

References

[1] Kaneko S, Ito T, Akiyama K, Yasui M, Kato C, Tanaka S, Hirabayashi Y, Mastuno A, Nire T and Funakubo H 2011 *Nanotechnology* **22** 175307
[2] Pang Z and Zhang X 2011 *Nanotechnology* **22** 145303
[3] Du K, Wathuthanthri I, Mao W, Xu W and Choi C H 2011 *Nanotechnology* **22** 285306
[4] Forsén E, Ghatnekar-Nilsson S, Carlberg P, Abadal G, Pérez-Murano F, Esteve J, Montserrat J, Figueras E, Campabadal F and Verd J 2004 *Nanotechnology* **15** S628
[5] Pena A A, Wang Z B, Zhang J, Wu N E and Li L 2011 *Nanotechnology* **22** 365302
[6] Kawata S, Sun H-B, Tanaka T and Takada K 2001 *Nature* **412** 697–8
[7] Juodkazis S, Mizeikis V and Misawa H 2009 *J. Appl. Phys.* **106** 051101
[8] Chen Z C, Hong M H, Lim C S, Han N R, Shi L P and Chong T C 2010 *Appl. Phys. Lett.* **96** 181101
[9] Lin S K, Yang P, Lin I C, Hsu H W and Tsai D P 2006 *Japan. J. Appl. Phys.* **45** 1431–4
[10] Ho F H, Chang H H, Lin Y H, Chen B M, Wang S Y and Tsai D P 2003 *Japan. J. Appl. Phys.* **42** 1000–4
[11] Yang C T, Chen C Y, Huang C C, Lee Y C, Chen S C and Cheng C T 2011 *IEEE Trans. Magn.* **47** 701–5
[12] Lin S K, Lin I C, Chen S Y, Hsu H W and Tsai D P 2007 *IEEE Trans. Magn.* **43** 861–3
[13] Lin S K, Lin I C and Tsai D P 2006 *Opt. Express* **14** 4452–8
[14] Srituravanich W, Pan L, Wang Y, Sun C, Bogy D B and Zhang X 2008 *Nature Nanotechnol.* **3** 733–7
[15] Vorobyev A Y, Makin V S and Guo C 2009 *Phys. Rev. Lett.* **102** 234301
[16] Malinauskas M, Danilevičius P and Juodkazis S 2011 *Opt. Express* **19** 5602–10
[17] Chichkov B N, Momma C, Nolte S, Von Alvensleben F and Tünnermann A 1996 *Appl. Phys.* A **63** 109–15
[18] Tseng M L, Chen B H, Chu C H, Chang C M, Lin W C, Chu N N, Mansuripur M, Liu A Q and Tsai D P 2011 *Opt. Express* **19** 16975–84
[19] Kuznetsov A I, Unger C, Koch J and Chichkov B N 2012 *Appl. Phys.* A **106** 479–87
[20] Kuznetsov A I, Kiyan R and Chichkov B N 2010 *Opt. Express* **18** 21198–203
[21] Bohandy J, Kim B F and Adrian F J 1986 *J. Appl. Phys.* **60** 1538–9
[22] Banks D P, Grivas C, Zergioti I and Eason R W 2008 *Opt. Express* **16** 3249–54
[23] Klini A, Loukakos P A, Gray D, Manousaki A and Fotakis C 2008 *Opt. Express* **16** 11300–9
[24] Willis D A and Grosu V 2005 *Appl. Phys. Lett.* **86** 244103
[25] Yang L, Wang C, Ni X, Wang Z, Jia W and Chai L 2006 *Appl. Phys. Lett.* **89** 161110
[26] Klini A, Loukakos P A, Gray D, Manousaki A and Fotakis C 2008 *Opt. Express* **16** 11300–9
[27] Serra P, Colina M, Fernández-Pradas J M, Sevilla L and Morenza J L 2004 *Appl. Phys. Lett.* **85** 1639–41
[28] Fogarassy E, Fuchs C, Kerherve F, Hauchecorne G and Perriere J 1989 *J. Appl. Phys.* **66** 457–9
[29] Toth Z and Szörényi T 1991 *Appl. Phys.* A **52** 273–9
[30] Chang-Jian S K, Ho J R, John Cheng J-W and Sung C K 2006 *Nanotechnology* **17** 1184–7
[31] Fardel R, Nagel M, Nuesch F, Lippert T and Wokaun A 2007 *Appl. Phys. Lett.* **91** 061103
[32] Kuznetsov A I, Evlyukhin A B, Goncalves M R, Reinhardt C, Koroleva A, Arnedillo M L, Kiyan R, Marti O and Chichkov B N 2007 *ACS Nano* **5** 4843–9
[33] Kuznetsov A I, Evlyukhin A B, Reinhardt C, Seidel A, Kiyan R, Cheng W, Ovsianikov A and Chichkov B N 2009 *J. Opt. Soc. Am.* B **26** B130–8
[34] Haynes C L, Young M A and Van Duyne R P 2001 *J. Phys. Chem.* B **105** 5599–611
[35] Lin W C, Huang S H, Chen C L, Chen C C, Tsai D P and Chiang H P 2010 *Appl. Phys.* A **101** 185–9
[36] Yin L, Vlasko-Vlasov V K, Pearson J, Hiller J M, Hua J, Welp U, Brown D E and Kimball C W 2005 *Nano Lett.* **5** 1399–402
[37] Jean-Claude W, Yvon L and Alain D 2003 *Phys. Rev.* B **68** 115401
[38] Chang C M, Chu C H, Tseng M L, Chiang H P, Mansuripur M and Tsai D P 2011 *Opt. Express* **19** 9492–504
[39] Chu C H, Tseng M L, Da Shiue C, Chen S W, Chiang H P, Mansuripur M and Tsai D P 2011 *Opt. Express* **19** 12652–7
[40] Chu C H, Shiue C D, Cheng H W, Tseng M L, Chiang H P, Mansuripur M and Tsai D P 2010 *Opt. Express* **18** 18383–9
[41] Shin H, Kim H, Lee H, Yoo H, Kim J and Lee M 2008 *Adv. Mater.* **20** 3457–61
[42] Zergioti I, Mailis S, Vainos N A, Ikiades A, Grigoropoulos C P and Fotakis C 1999 *Appl. Surf. Sci.* **138** 82–6
[43] Atwater H A and Polman A 2010 *Nature Mater.* **9** 205–13
[44] Liu Z, Hou W, Pavaskar P, Aykol M and Cronin S B 2011 *Nano Lett.* **11** 1111–6
[45] Chen J J, Wu J C S, Wu P C and Tsai D P 2011 *J. Phys. Chem.* C **115** 210–6
[46] Huang H J, Yu C P, Chang H C, Chiu K P, Chen H M, Liu R S and Tsai D P 2007 *Opt. Express* **15** 7132–9
[47] Drezet A, Hohenau A, Koller D, Stepanov A, Ditlbacher H, Steinberger B, Aussenegg F R, Leitner A and Krenn J R 2008 *Mater. Sci. Eng.* B **149** 220–9
[48] Chen W T, Chen C J, Wu P C, Sun S, Zhou L, Guo G Y, Hsiao C T, Yang K Y, Zheludev N I and Tsai D P 2011 *Opt. Express* **19** 12837–42
[49] Ditlbacher H, Hohenau A, Wagner D, Kreibig U, Rogers M, Hofer F, Aussenegg F R and Krenn J R 2005 *Phys. Rev. Lett.* **95** 257403
[50] Yang D-M, Huang C-C, Kao L-S, Lin C-C, Chi C-W, Lin H Y, Tsai D P, Lee C-H and Chiou A 2005 *Nanomed. Nanotechnol. Biol. Med.* **1** 286–92